Optimal Allocation of ESSs in Active Distribution Networks to Achieve their Dispatchability

Ji Hyun Yi, *Student Member, IEEE,* Rachid Cherkaoui, *Senior Member, IEEE,* and Mario Paolone, *Senior Member, IEEE*

***Abstract*—This paper presents a method for the optimal siting and sizing of energy storage systems (ESSs) in active distribution networks (ADNs) to achieve their dispatchability. The problem formulation accounts for the uncertainty inherent to the stochastic nature of distributed energy sources and loads. Thanks to the operation of ESSs, the main optimization objective is to minimize the dispatch error, which accounts for the mismatch between the realization and prediction of the power profile at the ADN connecting point to the upper layer grid, while respecting the grid voltages and ampacity constraints. The proposed formulation relies on the so-called Augmented Relaxed Optimal Power Flow (AR-OPF) method: it expresses a convex full AC optimal power flow, which is proven to provide a global optimal and exact solution in the case of radial power grids. The AR-OPF is coupled with the proposed dispatching control resulting in a two-level optimization problem. In the first block, the site and size of the ESSs are decided along with the level of dispatchability that the ADN can achieve. Then, in the second block, the adequacy of the ESS allocations and the feasibility of the grid operating points are verified over operating scenarios using the Benders decomposition technique. Consequently, the optimal size and site of the ESSs are adjusted. To validate the proposed method, simulations are conducted on a real Swiss ADN hosting a large amount of stochastic Photovoltaic (PV) generation.**

***Index Terms*—Active distribution networks, dispatchability, energy storage systems, optimal power flow, resource planning.**

NOMENCLATURE

Sets and Indices

l	Indices of buses and indices of lines connected upstream to the buses
$\mathcal{L}$	Set of buses excluding the slack bus and set of lines connected upstream to the buses
$\mathcal{L}^E$	Set of virtual buses connected to the real ESS candidate buses and set of virtual lines connected upstream to the virtual buses
$y \in \mathcal{Y}$	Indices and set of years
$d \in \mathcal{D}$	Indices and set of days
$t \in \mathcal{T}$	Indices and set of time intervals
$\phi \in \Phi_{dy}$	Indices and set of scenarios for day d and year y
$n \in \mathcal{N}$	Indices and set of benders iterations

Variables

$U_l \in \{0,1\}$	Installation status of the ESS at bus l
C_l	Energy reservoir of the ESS at bus l
R_l	Power rating of the ESS at bus l
$\tilde{p}_{ltdy}$	Average of the active load over all scenarios at: bus l, time t, day d, and year y
$\Delta p_{l\phi t}$	Deviation of prosumption for scenario ϕ and time t from $\tilde{p}_{ltdy}$
$\tilde{f}_{ltdy}$	Average of squared longitudinal current causing losses over all scenarios at: line l, time t, day d, and year y
$\Delta f_{l\phi t}$	Deviation of squared longitudinal current causing losses for scenario ϕ and time t from f_{ltdy}
DP_{tdy}	Dispatch plan associated with time t, day d, and year y at the grid connecting point (GCP)
$\epsilon_{l\phi t}$	Uncovered dispatch error at: bus l, scenario ϕ, and time t
$\theta_{\phi t}$	Leftover dispatch error rate for scenario ϕ, time t
$f_l \backslash \bar{f}_l$	Square of current magnitude causing losses in line l\Auxiliary upper bound variable
$v_l \backslash \bar{v}_l$	Square of voltage magnitude at bus l\Auxiliary upper bound variable
$s_l{=}p_l{+}jq_l$	Aggregated prosumption at bus l
$S_l^t{=}P_l^t{+}jQ_l^t$	Upstream complex power flow to line l
$\bar{S}_l^t{=}\bar{P}_l^t{+}j\bar{Q}_l^t$	Auxiliary variable of upstream complex power flow to line l (upper bound of S_l^t)
$\hat{S}_l^t{=}\hat{P}_l^t{+}j\hat{Q}_l^t$	Auxiliary variable of upstream complex power flow to line l (lower bound of S_l^t)
$S_l^b{=}P_l^b{+}jQ_l^b$	Downstream complex power flow to bus l from line l
$\bar{S}_l^b{=}\bar{P}_l^b{+}jQ_l^b$	Auxiliary variable of complex power flow to bus l from line l (upper bound of S_l^b)
$\hat{S}_l^b{=}\hat{P}_l^b{+}j\hat{Q}_l^b$	Auxiliary variable of complex power flow to bus l from line l (lower bound of S_l^b)
$s_l^E{=}p_l^E{+}jq_l^E$	Complex power flow of ESS at bus l
E_l^E	Energy stored in ESS installed at bus l
$ulp_{l\phi t}^{+}$	Positive unserved active load at: bus l, scenario ϕ, and time t
$ulp_{l\phi t}^{-}$	Negative unserved active load at: bus l, scenario ϕ, and time t
$ulq_{l\phi t}^{+}$	Positive unserved reactive load at: bus l, scenario ϕ, and time t
$ulq_{l\phi t}^{-}$	Negative unserved reactive load at: bus l, scenario ϕ, and time t
$\gamma_{\phi t}^{m}$	Slack variable for the realized losses deviation at m^{th} iteration of Alg. 1 for scenario ϕ and time t
$\zeta_{\phi t}$	Slack variable for the additional realization of losses deviation for scenario ϕ and time t

Parameters

T	Time horizon of the daily OPF problem
Δt	Time duration of dispatch interval
$\mathbf{H}$	Adjacency matrix
b_l	Half of the total shunt susceptance of line l
$z_l{=}r_l{+}jx_l$	Total longitudinal impedance of line l
I_l^{max}	Upper limit on the squared current of line l
$P_l^{max} \backslash Q_l^{max}$	Upper limits of active\reacitve power flows for line l, respectively
$v^{max} \backslash v^{min}$	Upper bounds\Lower bounds of the squared nodal voltage magnitude
SoE^{max}	Maximum allowed state-of-energy level
SoE^{min}	Minimum allowed state-of-energy level
SoE^{ini}	Initial state-of-energy level
λ_ϕ	Probability of scenario ϕ
$\mathcal{C}_l^{max} \backslash \mathcal{C}_l^{min}$	Maximum\minimum possible ESS energy reservoir capacity at bus l
$\mathcal{R}_l^{max} \backslash \mathcal{R}_l^{min}$	Maximum\minimum possible ESS power rating capacity at bus l
CR^{max}	Maximum power ramping rate of ESS
$\alpha_l, \beta_l, \kappa_l$	Vectors defining the slope and the inter-

	cepts, respectively, of the set of lines which approximate the power capability curve of ESS at bus l
N_c	Allowed number of cycles per day chosen as a function of the targeted ESS lifetime
$\mathcal{I}_c, \mathcal{I}_e, \mathcal{I}_p$	ESS investment costs associated to: fixed installation, energy reservoir, power rating
w_d, w_l, w_u	Weight coefficient associated to the error between the dispatch plan and the active slack power in each scenario, grid losses, unserved load, respectively
N_d	Number of days in each day-type in a year
r_{dis}	Discount rate
Y	Planning horizon

I. Introduction

POWER balancing is becoming an increasingly challenging task due to growing volatility in power systems introduced by the high penetration of non-dispatchable and stochastic distributed energy resources (DER). To be more specific, in the distribution grid, the prosumption forecast uncertainties are originated not only by the load consumption but also by the distributed renewable energy sources (RES). Thus, in these power grids, the deviation of the active power flow at the grid connecting point (GCP) from the prescheduled power intake from the upper grid, called *dispatch error*, should be compensated by the bulk system operating reserve. In this way, the spinning reserve requirement is growing to tackle not only the peak demand but also the stochasticity of *prosumption*[1], causing significant cost increases for transmission system operators (TSOs) to mitigate the system imbalance through the balancing mechanism. In this context, the central management of system imbalance may exhibit limitations and, several studies have called for the neccessity of modifying the market frameworks to encourage an appropriate cooperation between TSOs and distribution system operators (DSOs) to handle the system imbalance [1]. Furthermore, in [2], a reformation on the market framework is suggested to correctly allocate the balancing responsibility to the local DSOs based on the cost-causality principle. The new cost allocation scheme would highly incentivise DSOs to manage the prosumption uncertainty locally. In [3], it is studied how the so-called *dispatched by-design distribution networks* significantly reduce the reserve requirement for the bulk power system.

In this context, there has been increasing interest in using energy storage systems (ESSs) as a flexible resource to compensate for system imbalance [4], [5]. The European Network of Transmission System Operators for Electricity published a draft grid code addressing the possibility for ESSs to become a balancing serving providers [6]. However, the usage of ESSs is limited because system operators are, in general, not allowed to own or operate them under the current European power system regulatory framework. Yet, in [7], the Authors pointed out the neccessity and possibility to modify the regulatory framework regarding the ownership of ESSs to promote their further exploitation.

For this reason, in spite of the lack of an already established market and regulatory framework, in this paper we assume that: 1) a market environment with a modified regulatory framework allows system operators to invest on ESSs and to control them for balancing service but not for energy arbitrage; 2) the DSO is the financial representative for the imbalance caused within its active distribution network (ADN), which is penalized as an imbalance cost paid to the TSO. With the above assumptions, DSOs have enough motivation to integrate the ESSs to compensate the dispatch error, thereby enhancing the *dispatchability* of their ADNs and mitigate the aforementioned financial risk. The *dispatchability* identifies the capability of a resource, or a network, to control the realized active power flow through the resource, or the network, to follow a pre-defined power schedule with high fidelity.

There have already been studies addressing the optimal control strategies of ESSs to improve the dispatchability of the stochastic resource [8]–[10]. The Authors of [11] proposes an optimal control strategy of ESS to achieve the dispatchability of a distribution feeder. In day-ahead operation, the power schedule is computed following the prediction point of prosumption and the ESS is controlled such that the active power flow through the GCP tracks the power schedule with small deviation.

However, the efficient deployment of ESSs significantly depends on the investment planning. The problem of optimal siting and sizing of ESSs in ADNs has been already extensively investigated through numerous researches thanks to the versatile technical services that ESS can offer to DSOs such as: minimize network losses [12]–[14], provide voltage control [14]–[16], mitigate line congestion [14], and improve the quality of power supply [12], [17]. Moreover, several studies seek for the economic benefit from ESSs by providing ancillary service to TSOs [18] and focusing on minimizing operation cost [19]. Meanwhile, relatively few studies were dedicated to ESS planning for achieving dispatchability of ADNs.

The Authors of [20] and [21] proposed an algorithm to size a wind farm ESS to achieve its dispatchability. In [20], the ESS dispatch strategy is coupled with the assessment of its capacity and expected lifetime based on the confidence level of the power output w.r.t the predefined schedule. In [21], specific ESSs control algorithms are proposed along with a linear regression forecasting algorithm to compensate energy imbalance between the real power output and the predefined schedule of stochastic DERs. Furthermore, the impact of the balance service on the battery life is assessed. To ensure the economic optimality of decision-making, it is worth investigating the economic value of ESSs investments by taking into account their operational benefits and installation costs. There are few studies [22]–[25] addressing the financial risk of DSOs in the energy market regarding the imbalance caused within the ADNs. The work in [22] proposed a method for the optimal allocation of ESSs through a cost-benefit analysis, while integrating a control strategy of ESSs to compensate the gap between the actual prosumption and the purchased energy from the forward market, mitigating the DSO's risk in the real-time energy market. In [23], by using the same market framework as in [22], the Authors proposed the strategy of ESS planning and the optimal operation of DSOs considering the optimal bidding strategy in the day-ahead market and the optimal real-time operation of ESSs to minimize the imbalance cost. A similar objective was considered in [24] while considering distributed generation units along with ESSs. In [25], the ESSs capacity is determined for multiple agents, such as DSOs, wind farms, solar power stations and ADNs demand aggregators. The approach is based on the game theory with the objective to reduce the transaction cost risk of each agent due to the resources' forecast errors.

It is also worth observing that the capacity and placement of ESSs should comply with the characteristics of the chosen

[1]Prosumption is defined as the load consumption minus the locally generated power.

control strategy and the subsequent operational conditions of the system. In this regard, the optimal power flow (OPF) that accurately models operation and control of the ADN, should be embedded in the ESS planning tool. However, OPF-based ESSs planning is inherently burdensome to solve due to its non-convexity. There exists meta-heuristic methods such as fuzzy particle swarm optimization (PSO) algorithm used in [22] and [25], and PSO algorithm in [24]. However, these solution approaches cannot guarantee the global optimum or even a feasible solution. To tackle the non-convexity of the OPF problem, convexification approaches, such as the semi-definite programming (SDP) [26] or the second-order cone programming (SOCP) relaxation [15], [18], [19], [27], have emerged as a solid and rigorous alternative. The SOCP relaxation proposed in [28] has been implemented for the optimal ESS allocation in radial grids due to its superior computational efficiency referring to the SDP relaxation. In [18], an ESS planning strategy was developed relying on the SOCP-OPF model with the objective of providing ancillary services to the TSO, and to cope with the wind variability. The Authors of [19] further utilized the SOCP relaxed model for the ESSs allocation and operation to minimize the grid losses and imported power in the ADN. In [23], even though the optimization problem for day-ahead operation is modeled as a non-convex OPF problem and solved by implementing meta-heuristic evolution method, the optimization on the real-time operation is solved thanks to the relaxed SOCP based OPF model.

The work in [15] tackled the ESS planning and operation problem by decomposing it into two stages: first stage determines the total ESS size to prevent grid constraints violations due to PV power imbalance, and the second stage allocates ESSs with optimal sizes by employing SOCP-OPF to minimize the energy cost. Meanwhile, the Authors addressed that the objective function and constraints should satisfy some necessary conditions to guarantee the exactness of the SOCP-OPF solution, and suggested a formula to verify the exactness a-posteriori. The main drawbacks were explicitly underlined in [29] by the fact that the exactness of the solution cannot be guaranteed especially in the presence of reverse line power flows and for the cases where the upper bound of nodal voltage and the line ampacity constraints are binding. This brings significant limitations on the applicability of the method to ADNs hosting DERs with large capacities. Moreover, the model neglects the transverse elements of the lines, which can bring an infeasibility of the solution especially when ADNs are composed of coaxial underground cables. The work in [30] solves this problem and proposed the Augmented Relaxed OPF (AR-OPF) to convexify the AC-OPF for radial grids. Their contribution demonstrates that, in the AR-OPF problem comprising an objective function strictly increasing with the grid losses, the conditions for the exactness of the solution are mild and hold for realistic distribution networks. The AR-OPF was implemented in the subsequent works on the optimal ESS planning problem while embedding grid reconfiguration with the objective of minimizing grid losses, voltage deviation and the line congestion [14].

In this paper, we propose an operation-driven planning strategy of ESS to achieve the dispatchability of the ADN based on the AR-OPF model. The objective of achieving disatchability requires a substantial and non-trivial modification on the AR-OPF as well as on the solution approach proposed in [14] in order to reach the exactness of the relaxed OPF. Moreover, we formulated the sizing problem into two blocks by modifying the objective term, constraints and variables related to the dispatch error. Meanwhile, we apply the Benders decomposition to handle the multi-layered decisions with numerous scenarios [31]. The contributions of the paper are two as follows.

1) The optimal allocation of ESS is determined based on an exact convex model of the OPF to address the dispatchability of the ADN in the presence of prosumption uncertainty, while accurately reflecting the operational condition of the ADN.
2) The structure of the planning problem and the objective functions are formulated accounting for the necessary conditions to guarantee the optimality and the exactness of the OPF relaxation.

The paper is organised as follows: in Section II, we introduce the structure of the optimization problem and explain the key parts in detail. In Section III, the proposed problem formulation and solution approach are described. Section IV contains a detailed application example referring to the planning of ESSs into a real ADN. Finally, Section V concludes the paper.

II. Problem Structure

A. System Description

In this paper, optimal allocation of ESS is determined based on the operation of the ADN over the planning horizon Y, while the prosumption profiles are expected to grow each year with a constant rate. Each year indexed with $y \in \{1, ..., Y\} = \mathcal{Y}$, we classify days into day-types indexed with $d \in \mathcal{D}$. The uncertainty in prosumption in each day-type is represented by operating scenarios indexed with $\phi \in \Phi_{dy}$ with probability λ_ϕ for each scenario. The dispatch interval is identified by the index $t \in \{1, ..., T\} = \mathcal{T}$, where T corresponds to the scheduling horizon of the daily operation. Time indices are separated by a constant timestep Δt. The dispatch problem at day d accounts only for the active power. Each node of the ADN has a non-dispatchable aggregated prosumption ($s_{l\phi t}$) defined at each scenario and time interval. The aggregated ADN active powers through the GCP (which is equivalent to node 1) to an upper layer grid in all scenarios ($P_{1\phi t}, \forall \phi \in \Phi_{dy}$) are expected to follow a day-ahead determined daily dispatch plan at each time interval (DP_{tdy}) derived with the support of a forecasting tool. Then, at each node where an ESS is allocated (*i.e.*, $U_l = 1$, where $U_l \in \{0, 1\}$), it is dispatched at each scenario and time interval according to active power ($p^E_{l\phi t}$) and reactive power ($q^E_{l\phi t}$). The dispatched active power compensates for the gap between active power through the GCP and the dispatch plan, which results from the deviation of realized total prosumption from the total prosumption prediction. Consequently, the observed dispatch error at GCP can be minimized.

In summary, the ESS allocation problem to achieve the dispatchability of the ADN under study is a two-stage decision process: the first stage which deals with the binary decision variables on the location of the ESS (U_l) and the continuous decision variables on the capacity of the ESSs energy reservoirs (C_l) and their power rating (R_l), and the second stage which deals with daily dispatch problems, determining the decision variables on the ESSs active and reactive power for all operating scenarios.

B. Dispatch Plan of the Distribution Feeder

The operational benefit of ESSs allocation for the ADN dispatchability is evaluated with sets of operationg scenarios, where each set refers to a typical day. The set of day-types is supposed to be pre-selected by the modeler.

The advantage of using scenarios is related to the use of generic parametric and non-parametric distributions of prosumptions. In this paper, the active and reactive prosumption scenarios for each day are generated with the assumption that the prosumption profile follow a normal distribution. Therefore, the mean of the prosumption over the scenarios is equal to the given prosumption prediction, and the losses predictions are calculated by averaging the losses over the scenarios [11]. It is understood that the variables with subscript l, ϕ, t are defined for $l{\in}\mathcal{L}, \phi{\in}\Phi_{dy}, t{\in}\mathcal{T}$, respectively. In (3), a daily dispatch plan DP_{tdy} follows the predicted point of the total prosumption considering the predicted grid losses.

$$p_{l\phi t}{=}\tilde{p}_{ltdy}{-}\Delta p_{l\phi t}, \forall l, \forall \phi, \forall t \tag{1}$$

$$r_l f_{l\phi t}{=}r_l \tilde{f}_{ltdy}{-}r_l \Delta f_{l\phi t}, \forall l, \forall \phi, \forall t \tag{2}$$

$$DP_{tdy}{=}\sum_{l\in\mathcal{L}}(\tilde{p}_{ltdy}{+}r_l \tilde{f}_{ltdy}), \forall t \tag{3}$$

$P_{1\phi t}$ represents the active power through the GCP at each scenario and at time interval. In other words, it is the aggregate of all prosumption including the total grid losses in the ADN. In this context, the *dispatch error* with no dispatchable resources in ADN is formally defined as the total error of prosumption plus the line losses over the buses/lines as indicated in the left-hand side of (4). As in the right-hand side of (4), the installed ESSs in ADN can be dispatched with active power ($p^E_{l\phi t}$) to compensate for the error. $\epsilon_{l\phi t}$ represents the residual dispatch error that cannot be covered at bus l, scenario ϕ, and time t. To quantify the covered or not covered error by the ESSs, we say that the sum of the two parts, shown in the right-hand side of (4), is equal to the dispatch error in case of no dispatchable resources. Therefore, with ESS integrated in the ADN, the dispatch error at the GCP is expressed as (5).

$$\sum_{l\in\mathcal{L}}(\Delta p_{l\phi t}{+}r_l \Delta f_{l\phi t}){=}\sum_{l\in\mathcal{L}}(\epsilon_{l\phi t}{+}p^E_{l\phi t}), \forall \phi, \forall t \tag{4}$$

$$DP_{tdy} - P_{1\phi t}{=}\sum_{l\in\mathcal{L}}\epsilon_{l\phi t}, \forall \phi, \forall t \tag{5}$$

Finally, the objective term to minimize the power deviation from the daily dispatch plan for all scenarios and time intervals is expressed as follows.

$$\underset{p^E}{\text{minimize}} \sum_{t\in\mathcal{T}}\sum_{\phi\in\Phi_{dy}} \lambda_\phi \Big|\sum_{l\in\mathcal{L}}\epsilon_{l\phi t}\Big| \tag{6}$$

C. Augmented Relaxed Optimal Power Flow

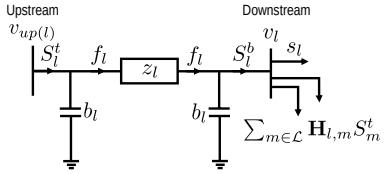

Fig. 1. Illustration of the adopted nomenclature with respect to the classic two-port Π model of a transmission line adopted from [30].

The description of the variables and parameters used in (7)-(22) is stated in the nomenclature. The above equations can be directly derived by applying the Kirchhoff's law to the two-port Π branch model shown in Fig. 1. For a radial power network, the power flow equations are given in (7)-(10). The variables with subscript l are defined for $l{\in}\mathcal{L}$. The upstream bus of bus l is notated as $up(l)$. $\mathbf{H}$ is the adjacency matrix of the network, where $\mathbf{H}_{k,l}$ is defined for $k, l{\in}\mathcal{L}$ and $\mathbf{H}_{k,l}{=}1$ if $k{=}up(l)$ or 0 if not. The line complex power S_l^t and S_l^b are determined by (7), and (8), respectively. The squared longitudinal current that produces losses at line l is originally defined as (10). By applying the SOCP relaxation, the equality is replaced with an inequality, as in (11) [28]. Hereafter, it is called as the relaxed OPF (R-OPF) model. Eq. (9) determines the magnitude of squared nodal voltages, where $\Re(.)$ represents the real parts of a complex number.

$$S_l^t{=}s_l{+}\sum_{m\in\mathcal{L}}\mathbf{H}_{l,m}S_l^t{+}z_l\, f_l{-}j(v_{up(l)}{+}v_l)b_l, \forall l \tag{7}$$

$$S_l^b{=}s_l{+}\sum_{m\in\mathcal{L}}\mathbf{H}_{l,m}S_l^t, \forall l \tag{8}$$

$$v_l{=}v_{up(l)}{-}2\Re\Big(z_l^*\Big(S_l^t{+}jv_{up(l)}b_l\Big)\Big){+}|z_l|^2 f_l, \forall l \tag{9}$$

$$f_l{=}\frac{|S_l^t + jv_{up(l)}b_l|^2}{v_{up(l)}}{=}\frac{|S_l^b - jv_l b_l|^2}{v_l}, \forall l \tag{10}$$

$$f_l \geq \frac{|S_l^t + jv_{up(l)}b_l|^2}{v_{up(l)}}, \forall l \tag{11}$$

In order to avoid any inexact solution of R-OPF model (*i.e.*, any solution that makes the left-hand side of (11) strictly greater than the right-hand side, and thus without physical meaning), the Authors of [30] introduced auxiliary variables $\bar{f}_l$, $\bar{S}_l{=}\bar{P}_l{+}j\bar{Q}_l$, $\bar{v}_l$ and $\hat{S}_l{=}\hat{P}_l{+}j\hat{Q}_l$ to formulate the AR-OPF model. The branch power flow, nodal voltage, and current equations are defined as well with the set of the auxiliary variables, as in (12)-(18). Eq. (12) and (13) indicate the lower bound of branch power flow at the sending end and the receiving end of line l. The upper bound nodal voltage is determined correspondingly with (14). Likewise, the branch power flow equations for upper bound power flow variables are shown as (15) and (16). Eq. (17) and (18) express that the upper bound of the squared longitudinal current f_l should be decided by the maximum of absolute complex power flow from both sides of line l. The voltage constraint, the ampacity constraint from the sending end and the receiving end are modeled as in (19)-(21). Eq (22) are added to complete the set of equations required to guarantee the exactness.

$$\hat{S}_l^t{=}s_l{+}\sum_{m\in\mathcal{L}}\mathbf{H}_{l,m}\hat{S}_l^t{-}j(\bar{v}_{up(l)}{+}\bar{v}_l)b_l, \forall l \tag{12}$$

$$\hat{S}_l^b{=}s_l{+}\sum_{m\in\mathcal{L}}\mathbf{H}_{l,m}\hat{S}_l^t, \forall l \tag{13}$$

$$\bar{v}_l{=}\bar{v}_{up(l)}{-}2\Re\Big(z_l^*(\hat{S}_l^t{+}j\bar{v}_{up(l)}b_l)\Big), \forall l \tag{14}$$

$$\bar{S}_l^t{=}s_l{+}\sum_{m\in\mathcal{L}}\mathbf{H}_{l,m}\bar{S}_l^t{+}z_l f_l{-}j(v_{up(l)}{+}v_l)b_l, \forall l \tag{15}$$

$$\bar{S}_l^b{=}s_l{+}\sum_{m\in\mathcal{L}}\mathbf{H}_{l,m}\bar{S}_l^t, \forall l \tag{16}$$

$$\begin{aligned}\bar{f}_l v_l \geq{}& |\max\big\{|\hat{P}_l^b|, |\bar{P}_l^b|\big\}|^2 \\ &{+}|\max\big\{|\hat{Q}_l^b{-}j\bar{v}_l b_l|, |\bar{Q}_l^b{-}jv_l b_l|\big\}|^2, \forall l\end{aligned} \tag{17}$$

$$\begin{aligned}\bar{f}_l v_{up(l)} \geq{}& |\max\big\{|\hat{P}_l^t|, |\bar{P}_l^t|\big\}|^2 \\ &{+}|\max\big\{|\hat{Q}_l^t{+}j\bar{v}_{up(l)}b_l|, |\bar{Q}_l^t{+}jv_{up(l)}b_l|\big\}|^2, \forall l\end{aligned} \tag{18}$$

$$v^{min} \leq v_l, \quad \bar{v}_l \leq v^{max}, \forall l \tag{19}$$

$$I_l^{max} v_{up(l)} \geq |\max\big\{|\hat{P}_l^t|, |\bar{P}_l^t|\big\}|^2{+}|\max\big\{|\hat{Q}_l^t|, |\bar{Q}_l^t|\big\}|^2, \forall l \tag{20}$$

$$I_l^{max} v_l \geq |\max\big\{|\hat{P}_l^b|, |\bar{P}_l^b|\big\}|^2{+}|\max\big\{|\hat{Q}_l^b|, |\bar{Q}_l^b|\big\}|^2, \forall l \tag{21}$$

$$\bar{P}_l^t \leq P_l^{max}, \qquad \bar{Q}_l^t \leq Q_l^{max}, \forall l \tag{22}$$

The nodal voltages and branches' ampacity constraints defined with the auxiliary variables (*i.e.*, (19)-(21)) construct

a conservative and convex set of constraints. The network model defined with (8)-(10) and (12)-(22) is called as the augmented-OPF (A-OPF), and its feasible set is proved to be a subset of the feasible set of original OPF. As already shown in [30], the set of grid constraints employing the auxiliary variables slightly shrinks the original feasible solution space in correspondence of undesirable operation points of the network (*e.g.*, near the upper bound of nodal voltages or branches' ampacity limits).[2]

The AR-OPF model is obtained by replacing (10) by (11). Under the pre-requisite conditions defined in [30], for every feasible solution of the AR-OPF, there exists a feasible solution of the A-OPF and also for the original OPF with the same power injection. Moreover, every optimal solution of the AR-OPF that satisfies (10) is an optimal solution of the A-OPF. It is noteworthy that (10) is satisfied in the AR-OPF model when the objective function is strictly increasing with respect to the squared longitudinal line current f_l, or the grid losses. The pre-requisite conditions to guarantee the exactness are defined with the grid parameters and they are mild enough to hold for general and realistic radial distribution networks. Since the Authors of [30] have rigorously proved all the statement above regarding the exactness of the AR-OPF solution [30], the readers are encouraged to refer to [30] for further details.

For the sake of readability, the equations mentioned above are grouped and represented by $\Theta(\varphi,\kappa)\geq 0$ where $\varphi=\{S^t, v, f, \hat{S}^t, \bar{v}, \bar{f}, \bar{S}^t, s\}$ is the set of variables and $\kappa=\{\mathbf{H}, z, b, v^{max}, v^{min}, I^{max}, P^{max}, Q^{max}\}$ is the set of parameters. The notation without subscript corresponds to the vector of variables and parameters for all buses/lines.

D. Energy Storage Systems

The ESS investment is modeled through (23)-(25). In reality, available power ratings and energy capacities are often restrained as in (23) and (24) due to various physical constraints involving, for instance, manufactural or geographical factors. CR^{max} is the maximum value for the rate at which ESS is discharged relatively to its maximum energy capacity. The power rating and energy reservoir is determined considering this relationship as in (25) (*e.g.*, we set $CR^{max}=3$ based on the typical maximum C-rate found in commercial BESSs).

$$\mathcal{R}_l^{min} U_l \leq R_l \leq R_l^{max} U_l, \forall l \tag{23}$$
$$\mathcal{C}_l^{min} U_l \leq C_l \leq \mathcal{C}_l^{max} U_l, \forall l \tag{24}$$
$$\Delta t R_l \leq \frac{C_l}{CR^{max}}, \forall l \tag{25}$$

In the 1st block problem (see Sec. III-A), we consider an ESS as an ideal battery. On the other hand, in the 2nd block problem (see Sec. III-B2), we model the ESS losses using the method proposed in [32], that is by adding an additional resistive lines (equivalent resistance[3] for the ESS losses) adjacent to the candidate nodes and treating them similarly as other lines in the AC-OPF. The resistance model is shown in Fig. 2. It should be noted that the positive sign of the ESS power denotes ESS charging power. The set of the virtual nodes corresponding to the additional lines is denoted as $\mathcal{L}^E$. For the virtual nodes, we introduce the ideal battery injection (in place of load injection) to the set of equations regarding AR-OPF model as $\Theta(\varphi^E,\kappa^E)\geq 0$, where $\varphi^E=\{S^t, v, f, \hat{S}^t, \bar{v}, \bar{f}, \bar{S}^t, s^E=p^E+jq^E\}$ is the set of variables and $\kappa^E=\{\mathbf{H}, z, b, v'^{max}, v'^{min}, I'^{max}, P^{max}, Q^{max}\}$[4] is the set of parameters. The notation without subscript corresponds to the vector of variables and parameters defined for $\forall l\in\mathcal{L}^E$. The operational characteristics of an ideal battery located at node $l\in\mathcal{L}^E$ are represented as (27)-(32). Eq. (26) refers to the ESS capability curve, which is approximated by a set of linear constraints inscribed within the original curve as in (27). α_l, β_l and κ_l are vectors defining the slope and the intercepts of the set of linear constraints. Eq. (28) expresses the ESS' state-of-energy (SoE) with charge/discharge power for each time interval. Eq. (29) indicates SoE limits on ESS operation during the day. As in (30), the initial SoE is set to be equal to SoE^{ini} (*e.g.*, we set $SoE^{ini}=50\%$) and the final SoE is set to be within $\pm 10\%$ of the initial SoE as in (31). Moreover, we account for the degradation of the ESS caused by its operation by (32). This constraint keeps ESS energy exchange within a threshold, which minimizes the cell deterioration during its daily operation [33]. ω is a positive parameter that depends on p_{lt}^E, and we chose the maximum value stated in [33] ($\omega=1$). N_c is the allowed number of cycles per day chosen as a function of the targeted ESS lifetime (*e.g.*, we set $N_c=0.96$ to model a typical ESSs according to [33]).

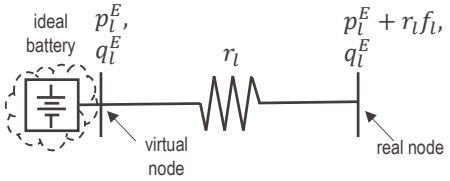

Fig. 2. The resistance model of battery adopted from [32].

$$(p_{lt}^E)^2 + (q_{lt}^E)^2 \leqslant R_l^2, \forall l, \forall t \tag{26}$$
$$\alpha_l p_{lt}^E + \beta_l q_{lt}^E \leqslant \kappa_l R_l, \forall l, \forall t \tag{27}$$
$$E_{l(t+1)}^E = E_{lt}^E + \Delta t p_{lt}^E, \forall l, \forall t \tag{28}$$
$$SoE^{min} C_l \leq E_{lt}^E \leq SoE^{max} C_l, \forall l, \forall t \tag{29}$$
$$E_{l(1)}^E = SoE^{ini} * C_l, \forall l, \forall t \tag{30}$$
$$E_{l(1)}^E - 0.1C_l \leq E_{l(T+1)}^E \leq E_{l(1)}^E + 0.1C_l, \forall l, \forall t \tag{31}$$
$$\frac{\Delta t}{2 * 1h} \left|\omega p_{lt}^E\right| \leq N_c C_l, \forall l, \forall t \tag{32}$$

In the interest of brevity, (27)-(32) are indicated by $\Xi(\eta,\xi)\geq 0, \forall t\in\mathcal{T}$ where $\eta=\{p^E, q^E, E^E, U, R, C\}$ is the set of variables and $\xi=\{\alpha, \beta, \kappa, \Delta t, SoE^{ini}, SoE^{min}, SoE^{max}, \omega, N_c\}$ is the set of parameters. The notation without subscript corresponds to the vectors of variables and parameters for $\forall l\in\mathcal{L}^E$.

III. Problem Formulation

The objective of the problem is to determine the optimal sizes and sites of ESSs so that the active power through the GCP follows the dispatch plan with minimal deviation. However, the dispatch error described by (6) in Sec. II-B does not increase while the total grid losses increase (a necessary

[2]We show that the compression of the solution space caused by the augmented constraints is small by following the steps of numerical analysis reported in [30]. Under the case study shown in Sec. IV, We make one of two operating constraints (voltage upper bound constraint and ampacity constraint) binding at one node or line and relax the other one to find the difference between the physical state variables (nodal voltage-magnitudes and original current flow) and corresponding auxilary variables. The difference between the nodal voltage-magnitude and the auxiliary one is 0.001%. The difference between the original current flow and the auxiliary one is equal to 0.2%.

[3]The resistances are updated in proportion to the ESS capacity using the reference value in [32]

[4]The value of $v'^{max}, v'^{min}, I'^{max}$ that apply to $\forall l\in\mathcal{L}^E$ are given such that the operating constraints regarding nodal voltage and line ampacity are not imposed to the buses/lines $\forall l\in\mathcal{L}^E$.

condition of the AR-OPF. See Sec. II-C). In order to verify this statement, we discuss the relationship between the dispatch error and the active power through the GCP instead of the grid losses, based on the fact that the active power through the GCP is strictly increasing with the grid losses [30]. The prediction error of the prosumption and the grid losses are random variables following normal distributions with zero mean value. Thus, it is obvious that the dispatch error, which is equivalent to the sum of prediction error of the prosumption and the grid losses over all buses/lines, is also a random variable with mean value of zero, and has neither positive nor negative correlation with the active power through GCP. Finally, the dispatch error does not have any correlation with the grid losses as well. Therefore, the exactness of the solution cannot be guaranteed if the objective value that corresponds to the objective term (6) is significant in magnitude compared to objective term regarding the total grid losses in the objective function of the AR-OPF model.

Therefore, we propose to decompose the problem into two blocks each consisting of an OPF problem. In this way, we can exclude (6) from the AR-OPF problem and convey it to another, approximated, OPF problem (the so-called 1st block problem), which aims to find the optimal level of dispatchability based on the ESSs investment cost and the imbalance penalty. The determined dispatchability level, defined as leftover dispatch error rate (LDER), is then introduced to an AR-OPF model-based problem (the so-called 2nd block problem) as an index which the ADN has to comply with.

The whole algorithm of the proposed approach is illustrated in Fig. 3. In the 1st block problem, the optimal ESSs allocation, the daily dispatch plans, and the corresponding LDER are calculated employing linear approximated OPF ignoring the grid losses. Only the nodal voltage constraints are considered regarding the operational constraints, ignoring the ampacity limits to reduce the computational burden. Afterward, the outputs of the 1st block, which are the ESS allocation and the LDER, are used as inputs for the 2nd block problem.

In the 2nd block problem, the objective is to refine the optimal allocation of the ESSs, considering several operating scenarios and achieving the same level of LDER calculated in the 1st block problem. In this respect, LDER is implemented as an additional constraint to an AR-OPF model, which considers the full AC-OPF as well as voltage constraints and branches' ampacity limits. Then, the size and site of the ESSs are iteratively adjusted thanks to the Benders decomposition technique. This iterative process starts initially with a feasibility check of the ESS allocation resulting from the 1st block problem.

A. 1st Block Problem

We minimize the investment and total penalty costs over the planning horizon to find out the optimal allocation of the ESSs and the optimal dispatchability level. We embed an approximated OPF constraints for all operating scenarios into a two-stage mixed-integer linear programming (MILP) problem (see Sec. II-A). The OPF is formulated by the linear Distflow model in which shunt elements are considered, whereas the grid losses are neglected. In this way, the reactive power generated by the shunt impedance of the lines is accounted for in the nodal voltage constraints. Meanwhile, neglecting the formulation of the squared longitudinal current (f_l) (*i.e.*, losses) is less likely to affect the feasible solutions in this stage since the ampacity constraint is ignored. The dispatch plan follows the prosumption prediction, as in (33), while the prosumption deviation at node l is expressed as in (34). We substitute (1) into the active power balance equation, resulting

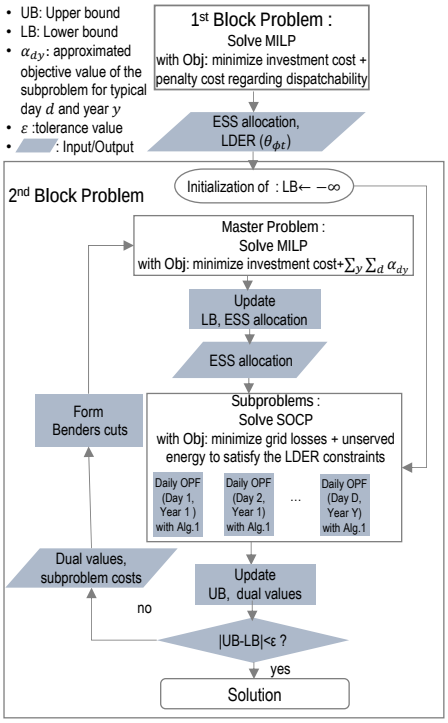

Fig. 3. Full algorithm of the proposed method.

in (35). The lossless Distflow power flow at both sides of line l including the ESS power are expressed via (35)-(37). Eq. (38) calculates the nodal voltage, which is governed by voltage constraint as in (39). All the variables within (34)-(39) are defined for $l\in\mathcal{L}$, $\phi\in\Phi_{dy}$, $t\in\mathcal{T}$, $d\in\mathcal{D}$, and $y\in\mathcal{Y}$. To simplify the notations, we do not show the indices for time, day, and year.

$$DP_{tdy}=\sum_{l\in\mathcal{L}}\tilde{p}_{ltdy},\forall t,\forall d,\forall y \tag{33}$$

$$\sum_{l\in\mathcal{L}}\Delta p_l=\sum_{l\in\mathcal{L}}(\epsilon_l+p_l^E),\forall\phi,\forall t,\forall d,\forall y \tag{34}$$

$$P_l^t=P_l^b=\tilde{p}_l-\Delta p_l+p_l^E+\sum_{m\in\mathcal{L}}\mathbf{H}_{l,m}\,P_l^t,\forall l,\forall\phi,\forall t,\forall d,\forall y \tag{35}$$

$$Q_l^t=q_l+q_l^E+\sum_{m\in\mathcal{L}}\mathbf{H}_{l,m}\,Q_l^t-(v_{up(l)}+v_l)b_l,\forall l,\forall\phi,\forall t,\forall d,\forall y \tag{36}$$

$$Q_l^b=q_l+q_l^E+\sum_{m\in\mathcal{L}}\mathbf{H}_{l,m}Q_l^t,\forall l,\forall\phi,\forall t,\forall d,\forall y \tag{37}$$

$$v_l=v_{up(l)}-2\Re\Big(z_l^*(S_l^t+jv_{up(l)}b_l)\Big),\forall l,\forall\phi,\forall t,\forall d,\forall y \tag{38}$$

$$v^{min}\le v_l\le v^{max},\forall l,\forall\phi,\forall t,\forall d,\forall y \tag{39}$$

The objective function is defined as to minimize the investment cost (the first line of (40)) of ESSs and the penalty cost (the second line of (40)) regarding the uncovered dispatch error over the planning horizon Y. The penalty cost of day d and year y is the uncovered dispatch error over the operating scenarios for day d multiplied by ω_d, which is the cost coefficient for the imbalance. Ω_1 and Ω_2 represents the set of control variables in the first and second stage decision process, respectively. The constraints regarding the ESS allocation and operation explained in Sec. II-D are included (*i.e.*, (23)-(25), (41)), along with the linear approximated lossless OPF constraints ((33)-(39)).

$$\underset{\substack{\forall U,C,R\in\Omega_1;\\ \forall S^t,v,s^E\in\Omega_2}}{\text{minimize}} \sum_{l\in\mathcal{L}}(\mathcal{I}_c U_l+\mathcal{I}_p R_l+\mathcal{I}_e C_l) + \sum_{y\in\mathcal{Y}} \frac{1}{(1+r_{dis})^y} \sum_{d\in\mathcal{D}} N_d w_d \sum_{t\in\mathcal{T}} \sum_{\phi\in\Phi_{dy}} \lambda_\phi |\sum_{l\in\mathcal{L}} \epsilon_{l\phi t}| \tag{40}$$

subject to: (23)-(25), (33)-(39),

$$\Xi(\eta_{\phi t},\xi)\geq 0,\ \forall\phi\in\Phi_{dy},\forall t\in\mathcal{T},\forall d\in\mathcal{D},\forall y\in\mathcal{Y} \tag{41}$$

Once the OPF problem including the constraints related to the dispatchability is solved, we can calculate the capability of the ADN with the allocated ESSs. In this context, we introduce a dispatchability index called LDER, and defined as $\theta_{\phi t}$. It is expressed in (42). It represents the ratio between the resulting dispatch error and the anticipated dispatch error in case of no ESS at scenario ϕ and time t for the daily operation on day d and year y (* here indicates that it is the identified optimal solution). In the denominator, the dispatch error without ESS is indicated while the error regarding the grid losses is ignored because its magnitude is negligible compared to that of the prosumption error.

$$\theta_{\phi t}=\frac{|\sum_{l\in\mathcal{L}} \epsilon^*_{l\phi t}|}{|\sum_{l\in\mathcal{L}} \Delta p_{l\phi t}|},\forall\phi\in\Phi_{dy},\forall t\in\mathcal{T},\forall d\in\mathcal{D},\forall y\in\mathcal{Y} \tag{42}$$

The two-stage MILP problem explained above can be easily tackled with numerous solvers such as GUROBI, MOSEK, etc. However, in the case where the sizes of the set $\Phi_{dy},\mathcal{D},\mathcal{Y}$ are significant, the size of the given MILP problem becomes too large-scaled to be handled by a commercial solver with limited computation power. In this regard, decomposition techniques (*e.g.*, benders decomposition, alternating direction method of multipliers method, etc.) can be employed as an effective solution approach to break down the first and the second stage of the optimization problem into two problems. Furthermore, the second-stage problem can be decomposed into several parallel problems such that the OPF problem for each day and each year can be tackled separately.

B. 2nd Block Problem

The dispatchability level is incorporated into the 2nd block problem as a constraint governed by the dispatchability index LDER. The objective of the 2nd block problem is to adjust the ESS allocation from the 1st block problem to the optimal site and size that can minimize the grid losses and unserved load. The system condition during the operation horizon is evaluated through solving the AR-OPF problem. Therefore, the 2nd block problem is formulated as a Mixed-integer second-order cone programming (MISOCP) problem. A convex SOCP model can be obtained from the non-convex MISOCP problem by using solution approaches that tackle the integer variables, such as the Branch and bound algorithm. However, the solution approach becomes computationally burdensome with the increase of integer variables. In this respect, we apply the Benders decomposition technique to decompose the 2nd block problem into a master problem and several parallel subproblems that each represents a daily OPF problem. The master problem determines the ESSs allocation, followed by the fitness evaluation of the determined allocations in the subproblems in terms of grid losses and unserved load. The unserved load takes values to ensure the feasibility of the subproblem regardless of the ESS allocation.

The initial step of the 2nd block is to solve parallel subproblems, checking the operational condition of ADN under the ESS allocation and the corresponding LDER calculated from the 1st block. The objective of the subproblem and the dual values of ESS allocation are computed and sent to the master problem to construct the first Bender's cut. Through multiple iterations between the master problems and the subproblems, the convergence is reached when the gap between the lower bound of the total cost (LB) and the upper bound of the total cost (UB) becomes less than a tolerance (the tolerance value is set as 0.01% of UB). LB is determined from the master problem, whereas UB is determined after solving subproblems.

1) Master Problem: The formulation of the master problem is given in (43). The master problem computes the lower bound of the planning problem by summing the investment cost and the lower approximation of the subsequent expected subproblem costs. Each α_{dy} represents the subproblem cost for days classified into each day type. It is initially bounded by $\underline{\alpha}$, which is the parameter given as the lower bound for the subproblem cost. In every nth iteration, Benders cuts represented by $\Gamma^{(n)}_{dy}$ (see (58)) are added as additional constraints for days $d\in\mathcal{D}$ and years $y\in\mathcal{Y}$, as in (44). The lowerbound of the total cost, so-called LB, is determined by the optimal solution of the master problem (*i.e.*, $LB=\mathcal{I}_c U^*_l+\mathcal{I}_p R^*_l+\mathcal{I}_e C^*_l+\sum_{y\in\mathcal{Y}}\sum_{d\in\mathcal{D}}\alpha^*_{dy}$).

$$\underset{\forall,U,C,R,\alpha}{\text{minimize}}\ \mathcal{I}_c U_l+\mathcal{I}_p R_l+\mathcal{I}_e C_l+\sum_{y\in\mathcal{Y}}\sum_{d\in\mathcal{D}}\alpha_{dy} \tag{43}$$

subjected to : (23)-(25),

$$\alpha_{dy}\geq\underline{\alpha},\ \alpha_{dy}\geq\Gamma^{(n)}_{dy},\ \forall d\in\mathcal{D},\forall y\in\mathcal{Y},\forall n\in\mathcal{N} \tag{44}$$

2) Subproblem: In the subproblem associated with day d, a daily AR-OPF model with the time-step discretization of Δt evaluates the operational advantages of ESSs while considering real operational conditions. The variables with subscript l,ϕ,t are defined for $l\in\mathcal{L},\phi\in\Phi_{dy},t\in\mathcal{T}$, respectively. The sufficiency of the ESS allocation is assessed by checking if the uncovered dispatch error (see (4)) satisfies the LDER for day d as in (45). As indicated in (46) and (47), we introduce positive and negative unserved active load terms ($ulp^+_{l\phi t},ulp^-_{l\phi t}\in\mathbb{R}^+$) and positive and negative unserved reactive load terms ($ulq^+_{l\phi t},ulq^-_{l\phi t}\in\mathbb{R}^+$) to the active prosumption and reactive prosumption at bus l, scenario ϕ and time t, respectively. They correspond to the amount that should be curtailed from the prosumption to primarily comply with the LDER constraint along with other operational constraints, even in the case of insufficient capacity of ESSs.

$$|\sum_{l\in\mathcal{L}}\epsilon_{l\phi t}|\leq\theta_{\phi t}|\sum_{l\in\mathcal{L}}\Delta p_{l\phi t}|,\ \forall\phi,\forall t \tag{45}$$

$$p'_{l\phi t}=p_{l\phi t}+ulp^+_{l\phi t}-ulp^-_{l\phi t},\ \forall l,\forall\phi,\forall t \tag{46}$$

$$q'_{l\phi t}=q_{l\phi t}+ulq^+_{l\phi t}-ulq^-_{l\phi t},\forall l,\forall\phi,\forall t \tag{47}$$

$$p'_{l\phi t}=\tilde{p'}_{ltdy}-\Delta p'_{l\phi t},\ \forall l,\forall\phi,\forall t \tag{48}$$

$$DP_{tdy}=\sum_{l\in\mathcal{L}}(\tilde{p'}_{ltdy}+r_l\tilde{f}_{ltdy}),\ \forall t \tag{49}$$

$$\sum_{l\in\mathcal{L}}(\Delta p'_{l\phi t}+r_l\Delta f_{l\phi t})=\sum_{l\in\mathcal{L}}\epsilon_{l\phi t}+\sum_{l\in\mathcal{L}^E}P^t_{l\phi t},\ \forall\phi,\forall t \tag{50}$$

The AR-OPF problem embedding the dispatchability for the subproblem is formulated by replacing (1) with (48). In other words, we replace the prosumption $p_{l\phi t}$ by $p'_{l\phi t}$ in the relevant equations. $\tilde{p'}_{ltdy}$ is employed in place of $\tilde{p}_{ltdy}$ to determine the daily dispatch plan, as in (49). $\Delta p_{l\phi t}$ of (4)

is substituted with $\Delta p'_{l\phi t}$ to build (50). The ESS power is expressed accounting for the battery losses. Similarly, $p'_{l\phi t}$ and $q'_{l\phi t}$ replace $p_{l\phi t}$ and $q_{l\phi t}$ in the active power balance equations formulated with the state variables (*i.e.*, (7), (8)) and the auxiliary variables (*i.e.*, (12), (13), (15), (16)). The equations of AR-OPF model are re-defined as (51), where $\varphi'=\{S^t, v, f, \hat{S}^t, \bar{v}, \bar{f}, \bar{S}^t, s'=p'+jq', ulp^+, ulp^-, ulq^+, ulq^-\}$ is the set of variables and $\kappa=\{\mathbf{H}, z, b, v^{max}, v^{min}, I^{max}, P^{max}, Q^{max}\}$ is the set of parameters. The notation without subscript corresponds to the vector of variables and parameters for buses/lines $\forall l\in\mathcal{L}$. Moreover, the power injection from the allocated ESS is introduced to the set of equations regarding AR-OPF model as in (52) (see Sec. II-D). The notation without subscript corresponds to the vector of variables and parameters for buses/lines $\forall l\in\mathcal{L}^E$. The ESS power is governed by the set of operational constraints as (53).

$$\Theta'(\varphi'_{\phi t}, \kappa)\geq 0, \forall\phi, \forall t \tag{51}$$

$$\Theta(\varphi^E_{\phi t}, \kappa^E)\geq 0, \forall\phi, \forall t \tag{52}$$

$$\Xi(\eta_{\phi t}, \xi)\geq 0,\ \forall\phi, \forall t. \tag{53}$$

However, we can intuitively expect that having (50) cannot be compliant with the mathematical formulation of the power flow equations (*i.e.*, (7)-(11)) in the case of insufficient capacity of ESS to satisfy the LDER constraint (45). The insufficient power rating of ESS means that possible $p^E_l, \forall l\in\mathcal{L}^E$ is small, and thus $P^t_{l\phi t}, \forall l\in\mathcal{L}^E$ is small. It makes ϵ_l too large to comply with LDER constraint (see (50)). However, instead of making the problem infeasible, LDER constraint and (50) are both satisfied by reducing the prosumption deviation considering losses (left-hand side of (50)). This leads to the violation of the physical law of power flow because the grid losses deviation should take an unrealistic value that has the same order of magnitude as the prosumption deviation. In this way, the prosumption deviation and grid losses deviation cancel out each other to make the overall value of the left-hand side as small as the right-hand side of (50). It would induce the increase of the squared longitudinal current f_l such that the left-hand side of (11) becomes strictly greater than the right-hand side, which leads to the inexactness of the solution. Therefore, we introduce an iterative algorithm, Alg. 1, comprising two additional slack variables, $\gamma^m_{\phi t}$ and $\zeta_{\phi t}$, to replace (50) by (54) and (55) such that the value of the internal current would never deviate away from the real value (*i.e.*, the exactness of the solution is guaranteed). $\gamma^m_{\phi t}$ represents the realized grid losses deviation at mth iteration for scenario ϕ and time t, where $m\in\mathcal{M}$ is the index of iterations of the algorithm. $\zeta_{\phi t}$ indicates the unrealized part of the grid losses that should be updated to $\gamma^m_{\phi t}$ after each iteration for scenario ϕ and time t. $\gamma^m_{\phi t}$ achieves the accurate value of grid losses deviation, as the absolute value of $\zeta_{\phi t}$ reaches value below the defined tolerance (we set the tolerance value as 1e-5 pu.).

$$\sum_{l\in\mathcal{L}}(\Delta p'_{l\phi t}+r_l\Delta f_{l\phi t})=\sum_{l\in\mathcal{L}}\epsilon_{l\phi t}+\sum_{l\in\mathcal{L}^E}P^t_{l\phi t},\ \forall\phi, \forall t \tag{54}$$

$$\sum_{l\in\mathcal{L}}\Delta p'_{l\phi t}+\gamma^m_{\phi t}=\sum_{l\in\mathcal{L}}\epsilon_{l\phi t}+\sum_{l\in\mathcal{L}^E}P^t_{l\phi t},\ \forall\phi, \forall t \tag{55}$$

Algorithm 1 Iterative realization of grid losses deviation

Input : $\theta(LDER), \kappa, s=p+jq, R^*, C^*$ (see (57))

1: **Initialization :** $m=1, \gamma^1=0, \zeta=1$;
2: **while** $|\zeta|\geq tolerance$ **do**
3: Solve a subproblem including (54) and (55)
4: $\gamma^{m+1}\leftarrow\gamma^m+\zeta$
5: $m\leftarrow m+1$
6: **end while**

Finally, the subproblem is described with an objective of minimization of the total grid losses and unserved load to satisfy the LDER constraint, and the operation period spans all days grouped into each day-type over the planning horizon.

$$\underset{\forall\varphi', \eta, UL}{\text{minimize:}}\ \mathcal{SC}_{dy}=\frac{1}{(1+r_{dis})^y}N_d\sum_{t\in\mathcal{T}}\sum_{\phi\in\Phi_{dy}}\lambda_\phi(w_l\sum_{l\in\mathcal{L}}r_l f_{l\phi t} + w_u\sum_{l\in\mathcal{L}}(ulp^+_{l\phi t}+ulp^-_{l\phi t}+ulq^+_{l\phi t}+ulq^-_{l\phi t})) \tag{56}$$

subject to: (45), (46), (47) (49), (52)-(55),

$$R_l=R^*_l:\mu_{ldy},\ C_l=C^*_l:\vartheta_{ldy},\ \forall l. \tag{57}$$

$$\Gamma^{(n)}_{dy}=\big[\mathcal{SC}^*_{dy}-\sum_{l\in\mathcal{L}}(\mu_{ldy}(R_l-R^*_l)-\vartheta_{ldy}(C_l-C^*_l))\big], \forall d, \forall y, \forall n \tag{58}$$

where $UL=\{ulp^+, ulp^-, ulq^+, ulq^-\}$ is the set of variables related to the unserved load. (57) describes that the ESS power ratings and the energy reservoirs are fixed to the optimal solution values of the master problem. μ_{ldy} and ϑ_{ldy} are the duals of constraints related to the fixed ESS capacities, and are used to form the benders cuts for the master problems as in (58). The variables with subscript d, y, n are defined for $\forall d\in\mathcal{D}, \forall y\in\mathcal{Y}, \forall n\in\mathcal{N}$, respectively. UB is calculated summing the optimal investment cost and the subproblem costs (*i.e.*, $UB=IC^*+\sum_{y\in\mathcal{Y}}\sum_{d\in\mathcal{D}}\mathcal{SC}^*_{dy}$).

IV. Simulation

We validate the performance of the proposed methods with an existing Swiss distribution network with 55 bus and large capacity of RES, as shown in Fig. 4. The base voltage is 21 kV and the base 3 phase power is 6 MVA. 2.7 MWp of PV generation capacity and 805 kVA of hydropower generation capacity is installed. The planning horizon is set as 10 years, and the annual growth rate of load consumption is considered as 3%. The discout rate r_{dis} is set as 7%. According to the indications of the operator of this grid, the number of candidate nodes for ESS installation is set as 5 out of 55 nodes (see Table I). In order to evaluate the impact of imbalance cost on the dispatchability, 3 representative values of imbalance costs analyzed from the imbalance price data from 2018 to 2019 in the Swiss energy market [34] (See Table II). The optimization problems are solved using the solver MOSEK via the MATLAB interface YALMIP.

TABLE I
ESS parameter and candidate nodes for simulation

Maximum power rating per site	3 MW	Maximum energy reservoir per site	4 MWh
Installation cost for energy reservoir	\$300/kWh	Installation cost for power rating	\$200/kVA
Capital investment cost per site		\$0.1 M	
Candidate nodes for ESS		4, 16, 27, 41, 45	

TABLE II
IMBALANCE PRICES FOR SIMULATION

	Imbalance price ($/MWh)
Mean	77
99th percentile	174
99.9th percentile	897

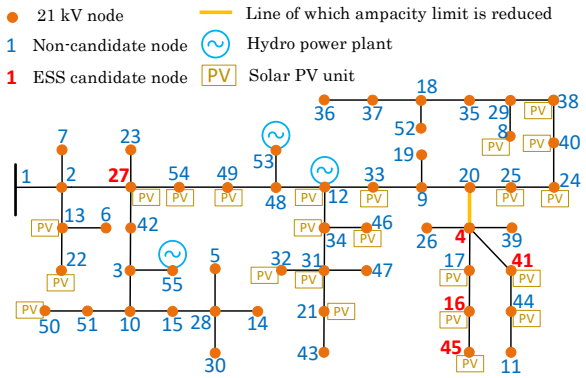

Fig. 4. Considered real 55 bus distribution feeder.

We consider 8 typical day-types to cover the seasonal variation of the prosumption over the year. For each day-type, we assume that prosumption forecasts for the simulation have been given from a reliable forecasting methodology. 1000 prosumption scenarios for each day are generated with equal probabilities based on the assumption that the prosumption profile follows a normal distribution as discussed in Sec. II-B. Then, we applied a K-medoids clustering [35] based scenario reduction technique to mitigate the computational burden. The number of reduced number of scenarios is determined by an algorithm explained in Appendix. A. However, it should be noted that it is a choice of the modeler.

A. Planning with 1 Day under Hourly Dispatch

To illustrate the role of the 1st and 2nd block of the problem, we demonstrate the result of the simplified simulation considering an hourly dispatch for 1 representative day in two cases: case 1 with the original ampacity of the lines specified for the given grid and case 2 with the ampacity of line between node 4 and 20 reduced from the original value (see Fig. 4). 32 representative scenarios obtained from the scenario reduction algorithm in Appendix. A are used as operating scenarios. Table III indicates the optimal allocation result of ESS, followed by the cost and operation result for 10 years as shown in Table IV. The optimal result from the 1st block specifies the capacity in size of power rating and energy reservoir of ESS. However, the determined allocation of ESS cannot be guaranteed to be feasible and optimal to satisfy the LDER for the real operation of the grid, since the grid losses and the ampacity constraint were neglected in the 1st block problem. After the 2nd block of the problem, as shown in the result of case 1 in Table III, the optimal site of the ESS considering the objective of minimization of the grid losses is determined as node 4, resulting in the reduction of the grid losses and unserved energy compared to the result of the 1st block problem.

In case 2, we can observe that a part of the load consumption was unserved to satisfy the LDER in the condition of restrained ampacity limit with the determined ESS allocation from the 1st block. In this regard, the result of the 2nd block shows the change in the allocation of the ESS due to the bottleneck of the line. The power rating and energy reservoir of the ESS on Node 4 is reduced, and another ESS is allocated on Node 27. Table IV shows that the unserved energy in case 2 decreased to near zero after re-allocating the ESS.

TABLE III
ESS ALLOCATION RESULT

Case	Problem	Location	Power rating	Energy reservoir
1	1st Block	41	564.3 kVA	1.615 MWh
	2nd Block	4	548.4 kVA	1.616 MWh
2	2nd Block	4	307.7 kVA	911.9 kWh
		27	238.7 kVA	705.4 kWh

TABLE IV
COMPARISON BETWEEN THE RESULT OF 1ST BLOCK AND 2ND BLOCK

Case	Type of cost	Allocation of 1st block	Allocation of 2nd block
case1	Investment cost ($ Million)	0.694	0.694
	Dispatch error (GWh)	2.037	2.037
	Unserved energy to satisfy the LDER (MWh)	0.086	2.7E-3
	Grid losses (MWh)	292.59	292.59
	Total energy consumed (GWh)	102.90	102.90
case2	Investment cost ($ Million)	0.694	0.794
	Dispatch error (GWh)	2.037	2.037
	Unserved energy to satisfy the LDER (MWh)	27.9	7.1E-4
	Grid losses (MWh)	306.30	281.85
	Total energy consumed (GWh)	102.92	102.89

B. Planning with Full Scenarios under 30 min Dispatch

The proposed planning procedure is applied to the full set of scenarios with 8 typical days under 30 min interval dispatch. We apply scenario reduction technique to 1000 scenarios of each day-type based on the algorithm in Appendix. A. The largest number of reduced scenarios over all day-types is determined as 39 scenarios. Table V shows the optimal ESS locations and sizes. We exhibit the results for three cases corresponding to different imbalance prices (see Table II). The cost and operation result for 10 years are indicated in Table VI. It signifies that it may not be beneficial to install ESSs under current imbalance prices (represented by the mean value of recorded imbalance prices). However, as the imbalance price grows higher with the increase of prosumption uncertainty within the system, it will be more necessary to allocate ESS for dispatch error compensation. Fig. 5 illustrates the operation result for day-type 1 in 1st year, showing the prosumption prediction considering 39 scenarios of the prosumption profiles (thick pink line), the dispatch plan (thick black line), and the active power infeed through GCP corresponding to each scenario (thin lines) in the case of no ESS (see Fig. 5.(a)) and the optimal ESS allocation with imbalance price of $897/MWh. (see Fig. 5.(b)). The dispatch result without ESS shows that the dispatch error is significant, especially in the time where the production from PV is high. On the other hand, in the case with the optimal ESS allocation, the active power infeed of every prosumption scenario follows the dispatch plan with small error. The cost analysis between the case with ESS and without ESS in Table VI demonstrates quantitatively the capability of ESS to handle uncertainties within the grid. When $897/MWh is considered for the imbalance price, the total dispatch error of the case without ESS is about 9 times of that in the case with ESS. The difference in the dispatch error is translated into the significant gap in the total cost for 10 years of operation: $12.45 Million with the default system configuration, and $2.54 Million with the optimal ESS allocation. Consequently, this result demonstrates the advantages for the DSO to invest on ESS in view of their technical and economical profit.

TABLE V
ESS ALLOCATION RESULT

Imbalance price	Location	Power rating	Energy reservoir
Mean	-	-	-
99th percentile	4	497.78 kVA	1.85 MWh
99.9th percentile	4 27	536.08 kVA 356.75 kVA	1.46 MWh 1.11 MWh

TABLE VI
COST AND OPERATIONAL BENEFITS

	Mean	99th percentile	99.9th percentile
Investment cost ($ Million)	-	0.75	1.15
Dispatch error (GWh)	13.875	2.881	1.552
Grid losses (MWh)	609.99	564.62	539.56
Unserved energy to satisfy the LDER (MWh)	0[1]	1.26	1.03
Total energy consumed (GWh)	104.84	104.77	104.77

[1] As the LDER is not calculated due to the lack of ESSs, the unserved energy is determined with only operating constraints regarding nodal voltage and ampacity limit.

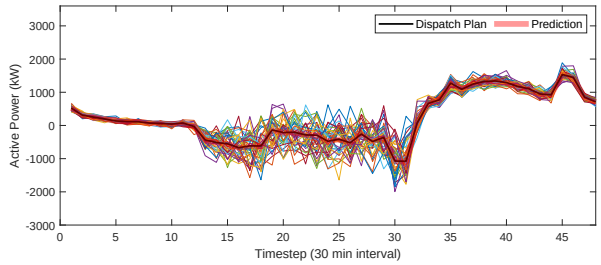

(a)

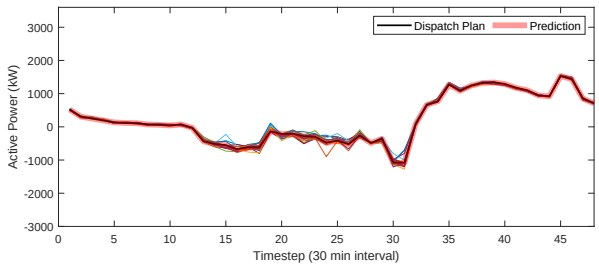

(b)

Fig. 5. Prosumption prediction, dispatch plan and active power through GCP in each scenario (not labeled for the sake of readability): (a) Day 1(No ESS), (b) Day 1(With ESS (Imbalance price : $897/MWh)).

C. Comparison with Planning Approach Using R-OPF Model

We compare the planning and operation results obtained from the proposed method with the AR-OPF model and with the R-OPF model [28]. The ESS allocation result along with the cost and operational benefits are shown in Table VII and Table VIII. The ESS allocation is quite similar with only a trivial difference in energy reservoir size, while the resulting dispatch error is same. The unserved energy to satisfy the LDER is smaller in the AR-OPF approach than R-OPF approach. Another comparison between two cases is analysed in terms of the exactness of the SOCP relaxation under the optimal allocation of ESS. The exactness is numerically evaluated based on the error between the right-hand side and the left-hand side of (11). The reference current value is 165 A. Table IX shows some of the statistic values that describe the distribution of the errors. The result verifies that AR-OPF model is superior to the R-OPF model concerning guaranteeing the exactness of the SOCP relaxation.

TABLE VII
ESS ALLOCATION RESULT USING AR-OPF AND R-OPF MODEL

Case	Location	Power rating	Energy reservoir
using AR-OPF	4	548.4 kVA	1.616 MWh
using R-OPF	4	548.2 kVA	1.659 MWh

TABLE VIII
COST AND OPERATIONAL BENEFITS USING AR-OPF AND R-OPF MODEL

	AR-OPF	R-OPF
Investment cost ($ Million)	0.694	0.707
Dispatch error (GWh)	2.037	2.036
Grid losses (MWh)	292.59	284.95
Unserved energy to satisfy the LDER (MWh)	0.086	1.759
Total energy consumed (GWh)	101.53	102.89

TABLE IX
ERROR IN LONGITUDINAL LINE CURRENT (A)

Case	median	95th percentile	99th percentile	99.9th percentile
using R-OPF	4.7E-3	3.1E-1	9.6E-1	4.1
using AR-OPF	6E-4	1.1E-2	2.5E-1	3.7E-1

D. Sensitivity Analysis on the Initial SoE

The results of dispatching operations are sensitive to the ESS operational condition. In the proposed planning method, only a few days are selected as typical day-types, and they are treated discontinuously for the operation. In Sec. II-D, the assumption on the initial and final SoE levels for each daily operation is discussed. In this sensitivity analysis, the initial SoE is chosen with various values to observe whether it plays a significant role in quantifying the optimal dispatchability level of ADNs, and ultimately influencing the size of ESSs. Table X, Table XI indicate the ESS allocation and cost result with different initial SoE conditions. The dispatch error in case of an initial SoE=50% appears to be the largest. However, when the sum of investment cost and the cost related to the dispatch error are compared for all cases, the results show that setting the initial SoE=50% gives the most economic ESS allocation.

TABLE X
ESS ALLOCATION RESULT WITH DIFFERENT INITIAL SOE LEVELS

Initial SoE	Location	Power rating	Energy reservoir
30%	4	507.7 kWh	2.218 MWh
50%	4	548.4 kVA	1.616 MWh
70%	4	631.1 kVA	2.052 MWh

TABLE XI
COST AND OPERATIONAL BENEFITS WITH DIFFERENT INITIAL SOES

	30 %	50 %	70 %
Investment cost ($ Million)	0.867	0.694	0.842
Dispatch error (GWh)	1.995	2.037	1.964
Grid losses (MWh)	292.63	292.59	293.26
Unserved energy to satisfy the LDER (MWh)	4.9E-3	0.086	2.3E-3
Total energy consumed (GWh)	103.01	101.53	102.81

V. DISCUSSION ON THE LIMITATION OF THE RESEARCH

Modeling the prosumption uncertainty can affect the fidelity of the optimal solution regarding the allocation of ESS and the dispatchabiliy level of an ADN. However, as modeling of prosumption stochasticity is not the scope of this paper, the prosumption scenarios are generated simply assuming that the prosumption follows a normal distribution. Nevertheless, when a modeler is equiped with a robust scenario generator which

models accurately the prosumption uncertainty, the proposed approach can guarantee the reliable performance. Another limitation of the proposed approach relates to the condition on the objective function for guaranteeing the exactness of the solution. This condition may limit the extendibility of the application for various control objectives of DSO's interest. For example, the minimization of the voltage deviation or control on ESS energy level may not satisfy the condition for the exactness, and having these objective terms within the objective function may affect the quality of the solution. Therefore, appropriate modification on the AR-OPF model would be necessary corresponding to such control objectives.

VI. Conclusion

In this study, we have presented a tool for the optimal planning of ESSs within a distribution network to achieve its dispatchability. We have shown that the uncertainty of the prosumption can be compensated sufficiently with the allocation and exploitation of ESS. The non-approximated and convex OPF model, or the AR-OPF model is implemented to account for the operational conditions of the distribution network accurately. The planning problem is decomposed into two blocks to satisfy the condition for the exactness of the solution via the AR-OPF model. In the 1st block, the allocation of ESS is determined along with the corresponding LDER by implementing the linearly approximated OPF model. The AR-OPF is used in the 2nd block of the problem to check the compatibility of the allocated capacity for the real operation of the grid to satisfy the LDER and to determine the optimal location of the ESS to minimize the grid losses. We validated the effectiveness of the proposed method for a real Swiss ADN of 55 nodes by demonstrating that the allocation of ESS successfully reduced the dispatch error.

VII. Acknowledgement

This project is carried out within the frame of the Swiss Centre for Competence in Energy Research on the Future Swiss Electrical Infrastructure (SCCER-FURIES) with the financial support of the Swiss Innovation Agency (Innosuisse - SCCER program) and ABB Corporate Research, Switzerland.

Appendix A
Scenario Reduction Algorithm

Scenario reduction techniques are typically applied to select a subset of initial scenario set. The quality of a stochastic optimization solution highly depends on how much the scenarios in the subset can properly preserve the probabilistic properties of the origianl scenario set. There have been specific studies on the scenario reduction where the minimum number of reduced scenarios is usually identified a-posteriori by observing the converging trend of the objective value with different number of reduced scenarios (*e.g.* [36]). However, for the sake of simplicity, we adopted the algorithm shown in Alg. 2 to a-priori obtain the minimum number of reduced scenarios that can approximate the distribution function of the uncertainty. Each of the generated scenarios is expressed as vector $\boldsymbol{\nu}_\phi = \{\nu_\phi^1, ..., \nu_\phi^H\}, \forall \phi \in \Phi_{dy}$ where $H = \sum_{l\in\mathcal{L}}(T^{AL(l)} + T^{RL(l)} + T^{PV}$. $T^{AL(l)}, T^{RL(l)}$, and T^{PV} are the time duration of the daily active, reactive load at node l, and PV irradiation profiles, respectively. Firstly, we construct a cumulative distribution function (CDF) for each random variable $\boldsymbol{\nu}^h$ with scenario set Φ_{dy}, which is given by $y_\phi^h = cdf(\nu_\phi^h) = P(\boldsymbol{\nu}^h \le \nu_\phi^h), \forall \phi \in \Phi_{dy}, h \in \{1, ..., H\} = \mathcal{H}$. $cdf^{-1}(y_\phi^h), y_\phi^h \in [0, 1]$ represents its inverse function. The obejctive of the algorithm is to find the minimal number of reduced scenarios such that the average distance between the CDF of the initial scenario set and that of the reduced scenario set over number of check points becomes smaller than a given tolerance. We define the check points for caclulating the distance between the CDF curve of scenario set Φ_{dy} with another CDF curve as $cdf^{-1}(y_{\Phi_{dy}}(q)), y_{\Phi_{dy}}(q) \in [0, 1], \forall q \in \{1, ..., N_q\}$. In this paper, we selected $N_q = 5$, with quantiles ranging $[0.05, 0.95]$. The scenario reduction process is initialized by applying K-Medoids clustering method [35] based on the Euclidean distance between each scenario pairs to reduce the original scenario set into set Φ'_{dy} with a single representative scenario. The average distance between CDFs of different scenario set Φ_{dy} and Φ'_{dy} is calculated by index defined by $\Delta = \sum_q \omega_q \sqrt{\frac{1}{H}\sum_h \left(\frac{cdf^{-1}(y^h_{\Phi_{dy}}(q)) - cdf^{-1}(y^h_{\Phi'_{dy}}(q))}{cdf^{-1}(y^h_{\Phi_{dy}}(q))} \right)^2}$, where ω_q is the weight coefficient assigned to qth check point. As the distance is bigger than a threshold value, the scenario reduction is re-applied to produce a scenario set with incremented number of scenarios than the previous iteration. Fig. 6(a) shows a CDF of original scenario set with the CDFs of different reduced scenario sets regarding a single random variable. The proposed algorithm determines that the minimum number of scenarios required is 39. Fig. 6(b) shows the evolution of Δ w.r.t the number of reduced scenarios.

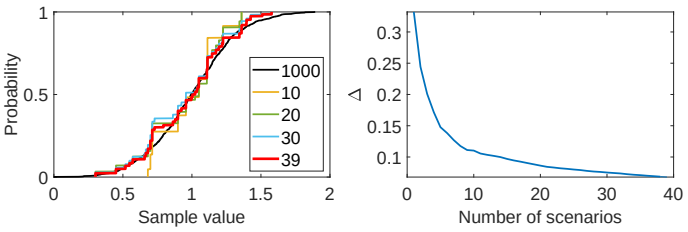

(a) (b)

Fig. 6. (a) CDF of initial scenario set and reduced scenario sets with different number of reduced scenarios, (b) Average of normalized distance between initial and reduced scenario sets with different number of reduced scenarios

Algorithm 2 Scenario reduction

1: Generate $N_{\Phi_{dy}}$ scenarios for $\boldsymbol{\nu}$
2: Draw CDF graphs of $\boldsymbol{\nu}^h, \forall h \in \mathcal{H}$ with scenario set Φ_{dy}.
3: **Initialization:** $N_{\Phi'_{dy}} = 0, \Delta = \infty$
4: **while** $|\Delta| \ge tolerance$ **do**
5: $N_{\Phi'_{dy}} \leftarrow N_{\Phi'_{dy}} + 1$
6: Obtain $N_{\Phi'_{dy}}$ scenarios for $\boldsymbol{\nu}$ via K-medoids clustering
7: Draw CDF graphs of $\boldsymbol{\nu}^h, \forall h \in \mathcal{H}$ with scenario set Φ'_{dy}.
8: Compute Δ between the two CDFs of set Φ_{dy} and Φ'_{dy}.
9: **end while**
10: **return** $N_{\Phi'_{dy}}, \boldsymbol{\nu}_{\phi'}, \forall \phi' \in \Phi'_{dy}$

References

[1] S. Lavrijssen, A.-A. Marhold, and A. Trias, "The changing world of the dso in a smart energy system environment: Key issues and policy recommendations," 2016.

[2] S. Kim, M. Pollitt, Y. Jin, J. Kim, and Y. Yoon, "Contractual framework for the devolution of system balancing responsibility from the transmission system operator to distribution system operators," 2017.

[3] M. Bozorg, F. Sossan, J.-Y. Le Boudec, and M. Paolone, "Influencing the bulk power system reserve by dispatching power distribution networks using local energy storage," *Electric Power Systems Research*, vol. 163, pp. 270–279, 2018.

[4] Y. V. Makarov, P. Du, M. C. Kintner-Meyer, C. Jin, and H. F. Illian, "Sizing energy storage to accommodate high penetration of variable energy resources," *IEEE Transactions on sustainable Energy*, vol. 3, no. 1, pp. 34–40, 2011.

[5] H.-I. Su and A. El Gamal, "Modeling and analysis of the role of energy storage for renewable integration: Power balancing," *IEEE Transactions on Power Systems*, vol. 28, no. 4, pp. 4109–4117, 2013.

[6] A. ENTSO-E, "Entso-e network code on electricity balancing," 2014.

[7] S. Ugarte, J. Larkin, B. Van der Ree, V. Swinkels, M. Voog, N. Friedichsen, J. Michaels, A. Thielmann, M. Wietschel, and R. Villafafila, "Energy storage: which market designs and regulatory incentives are needed," *European Parliament Committee on Industry, Research and Energy: Brussels, Belgium*, pp. 1–5, 2015.

[8] E. Perez, H. Beltran, N. Aparicio, and P. Rodriguez, "Predictive power control for pv plants with energy storage," *IEEE Trans. Sustain. Energy*, vol. 4, no. 2, pp. 482–490, April 2013.

[9] R. R. Appino, J. Á. G. Ordiano, R. Mikut, T. Faulwasser, and V. Hagenmeyer, "On the use of probabilistic forecasts in scheduling of renewable energy sources coupled to storages," *Applied energy*, vol. 210, pp. 1207–1218, 2018.

[10] G. Koeppel and M. Korpås, "Improving the network infeed accuracy of non-dispatchable generators with energy storage devices," *Electr. Pow. Syst. Res.*, vol. 78, no. 12, pp. 2024–2036, 2008.

[11] F. Sossan, E. Namor, R. Cherkaoui, and M. Paolone, "Achieving the dispatchability of distribution feeders through prosumers data driven forecasting and model predictive control of electrochemical storage," *IEEE Trans. Sustain. Energy*, vol. 7, no. 4, pp. 1762–1777, Oct 2016.

[12] H. Doagou-Mojarrad, G. Gharehpetian, H. Rastegar, and J. Olamaei, "Optimal placement and sizing of dg (distributed generation) units in distribution networks by novel hybrid evolutionary algorithm," *Energy*, vol. 54, pp. 129–138, 2013.

[13] J. Xiao, Z. Zhang, L. Bai, and H. Liang, "Determination of the optimal installation site and capacity of battery energy storage system in distribution network integrated with distributed generation," *IET Gener. Transm. Distrib.*, vol. 10, no. 3, pp. 601–607, 2016.

[14] M. Nick, R. Cherkaoui, and M. Paolone, "Optimal planning of distributed energy storage systems in active distribution networks embedding grid reconfiguration," *IEEE Trans. Power Syst.*, vol. 33, no. 2, pp. 1577–1590, March 2018.

[15] Q. Li, R. Ayyanar, and V. Vittal, "Convex optimization for des planning and operation in radial distribution systems with high penetration of photovoltaic resources," *IEEE Trans. Sustain. Energy*, vol. 7, no. 3, pp. 985–995, 2016.

[16] M. Nick, M. Hohmann, R. Cherkaoui, and M. Paolone, "On the optimal placement of distributed storage systems for voltage control in active distribution networks," in *2012 3rd IEEE PES Innov. Smart Grid Technol. Eur.* IEEE, 2012, pp. 1–6.

[17] G. Carpinelli, F. Mottola, D. Proto, A. Russo, and P. Varilone, "A hybrid method for optimal siting and sizing of battery energy storage systems in unbalanced low voltage microgrids," *Applied Sciences*, vol. 8, no. 3, p. 455, 2018.

[18] M. Qin, K. W. Chan, C. Y. Chung, X. Luo, and T. Wu, "Optimal planning and operation of energy storage systems in radial networks for wind power integration with reserve support," *IET Gener. Transm. Distrib.*, vol. 10, no. 8, pp. 2019–2025, 2016.

[19] E. Grover-Silva, R. Girard, and G. Kariniotakis, "Optimal sizing and placement of distribution grid connected battery systems through an socp optimal power flow algorithm," *Applied Energy*, vol. 219, pp. 385–393, 2018.

[20] Q. Li, S. S. Choi, Y. Yuan, and D. Yao, "On the determination of battery energy storage capacity and short-term power dispatch of a wind farm," *IEEE Trans on Sustain. Energy*, vol. 2, no. 2, pp. 148–158, April 2011.

[21] X. Ke, N. Lu, and C. Jin, "Control and size energy storage systems for managing energy imbalance of variable generation resources," *IEEE Transactions on Sustainable Energy*, vol. 6, no. 1, pp. 70–78, 2014.

[22] Y. Zheng, Z. Y. Dong, F. J. Luo, K. Meng, J. Qiu, and K. P. Wong, "Optimal allocation of energy storage system for risk mitigation of discos with high renewable penetrations," *IEEE Trans. Power Syst.*, vol. 29, no. 1, pp. 212–220, Jan 2014.

[23] Y. Zheng, J. Zhao, Y. Song, F. Luo, K. Meng, J. Qiu, and D. J. Hill, "Optimal operation of battery energy storage system considering distribution system uncertainty," *IEEE Transactions on Sustainable Energy*, vol. 9, no. 3, pp. 1051–1060, 2017.

[24] J. Qiu, Z. Xu, Y. Zheng, D. Wang, and Z. Y. Dong, "Distributed generation and energy storage system planning for a distribution system operator," *IET Renewable Power Generation*, vol. 12, no. 12, pp. 1345–1353, 2018.

[25] Y. Zheng, D. J. Hill, and Z. Y. Dong, "Multi-agent optimal allocation of energy storage systems in distribution systems," *IEEE Trans on Sustain. Energy*, vol. 8, no. 4, pp. 1715–1725, 2017.

[26] A. Giannitrapani, S. Paoletti, A. Vicino, and D. Zarrilli, "Optimal allocation of energy storage systems for voltage control in lv distribution networks," *IEEE Trans. Smart Grid*, vol. 8, no. 6, pp. 2859–2870, 2016.

[27] M. Nick, R. Cherkaoui, and M. Paolone, "Optimal allocation of dispersed energy storage systems in active distribution networks for energy balance and grid support," *IEEE Transs on Power Syst.*, vol. 29, no. 5, pp. 2300–2310, Sep. 2014.

[28] R. A. Jabr, "Radial distribution load flow using conic programming," *IEEE Trans. Power Syst.*, vol. 21, no. 3, pp. 1458–1459, 2006.

[29] K. Christakou, D.-C. Tomozei, J.-Y. L. Boudec, and M. Paolone, "Ac opf in radial distribution networks part i: On the limits of the branch flow convexification and the alternating direction method of multipliers," *Electr. Pow. Syst. Res.*, vol. 143, pp. 438 – 450, 2017.

[30] M. Nick, R. Cherkaoui, J. L. Boudec, and M. Paolone, "An exact convex formulation of the optimal power flow in radial distribution networks including transverse components," *IEEE Trans. Autom. Control*, vol. 63, no. 3, pp. 682–697, March 2018.

[31] A. M. Geoffrion, "Generalized benders decomposition," *J. Optimiz. Theory App.*, vol. 10, no. 4, pp. 237–260, 1972.

[32] E. Stai, L. Reyes-Chamorro, F. Sossan, J.-Y. Le Boudec, and M. Paolone, "Dispatching stochastic heterogeneous resources accounting for grid and battery losses," *IEEE Transactions on Smart Grid*, vol. 9, no. 6, pp. 6522–6539, 2017.

[33] E. Namor, D. Torregrossa, F. Sossan, R. Cherkaoui, and M. Paolone, "Assessment of battery ageing and implementation of an ageing aware control strategy for a load leveling application of a lithium titanate battery energy storage system," in *2016 IEEE 17th Workshop on Control and Modeling for Power Electronics (COMPEL)*. Ieee, 2016, pp. 1–6.

[34] (2020) The prices for balance energy in swissgrid. [Online]. Available: https://www.swissgrid.ch/en/home/customers/topics/bgm/balance-energy.html

[35] A. K. Jain and R. C. Dubes, *Algorithms for clustering data*. Prentice hall Englewood Cliffs, NJ, 1988, vol. 6.

[36] J. Hu and H. Li, "A new clustering approach for scenario reduction in multi-stochastic variable programming," *IEEE Transactions on Power Systems*, vol. 34, no. 5, pp. 3813–3825, 2019.

Ji Hyun Yi received the B.Sc. degree in electrical and electronic engineering from Yonsei University, South Korea, in 2015. Then, she received the M. Sc. Degree in electrical engineering from the National University of Seoul in 2018. She is currently a PhD student at the Distributed Electrical Systems Laboratory of the Swiss Federal Institute of Technology Lausanne (EPFL). Her research interests include distribution system planning for procurement of local system flexibility.

Rachid Cherkaoui (Senior Member, IEEE) received the M.Sc. and Ph.D. degrees in electrical engineering from the Swiss Federal Institute of Technology in Lausanne (EPFL), Lausanne, Switzerland, in 1983 and 1992, respectively. He is currently a Senior Scientist with EPFL, leading the Power Systems Group. He has authored and coauthored more than 150 scientific publications. His research interests include electricity market deregulation, distributed generation and storage, and power system vulnerability mitigation. Dr. Cherkaoui is a member of technical program committees of various conferences and was a member of CIGRE TFs and WGs. He was the IEEE Swiss Chapter Officer from 2005 to 2011.

Mario Paolone (M07SM10) received the M.Sc. (Hons.) and Ph.D. degrees in electrical engineering from the University of Bologna, Italy, in 1998 and 2002. In 2005, he was an Assistant Professor in power systems with the University of Bologna, where he was with the Power Systems Laboratory until 2011. Since 2011, he has been with the Swiss Federal Institute of Technology, Lausanne, Switzerland, where he is currently Full Professor and the Chair of the Distributed Electrical Systems Laboratory. His research interests focus on power systems with particular reference to real-time monitoring and operation aspects, power system protections, dynamics and transients. Dr. Paolone has authored or coauthored over 300 papers published in mainstream journals and international conferences in the area of energy and power systems that received numerous awards including the 2013 IEEE EMC Technical Achievement Award, two IEEE Transactions on EMC best paper awards and the Basil Papadias best paper award at the 2013 IEEE PowerTech. Dr. Paolone was the founder Editorin-Chief of the Elsevier journal Sustainable Energy, Grids and Networks.